

Sensitivity of Southern Ocean circulation to wind stress changes: Role of relative wind stress

D.R. Munday^{a,b,*}, X. Zhai^{c,d}

^a*British Antarctic Survey, High Cross, Madingley Road, Cambridge, CB3 0ET, UK*

^b*Atmospheric, Oceanic and Planetary Physics, Department of Physics, University of Oxford, Oxford, OX1 3PU, UK*

^c*School of Environmental Sciences, University of East Anglia, Norwich, UK.*

^d*School of Marine Science, Nanjing University of Information Science and Technology, Nanjing, China.*

Abstract

The influence of different wind stress bulk formulae on the response of the Southern Ocean circulation to wind stress changes is investigated using an idealised channel model. Surface/mixed layer properties are found to be sensitive to the use of the relative wind stress formulation, where the wind stress depends on the difference between the ocean and atmosphere velocities. Previous work has highlighted the surface eddy damping effect of this formulation, which we find leads to increased circumpolar transport. Nevertheless the transport due to thermal wind shear does lose sensitivity to wind stress changes at sufficiently high wind stress. In contrast, the sensitivity of the meridional overturning circulation is broadly the same regardless of the bulk formula used due to the adiabatic nature of the relative wind stress damping. This is a consequence of the steepening of isopycnals offsetting the reduction

*Corresponding author

Email addresses: danday@bas.ac.uk (D.R. Munday), xiaoming.zhai@uea.ac.uk (X. Zhai)

in eddy diffusivity in their contribution to the eddy bolus overturning, as predicted using a residual mean framework.

Keywords: Ocean modelling, Relative wind stress, Wind forcing, Eddy saturation, Eddy Compensation

¹ 1. Introduction

² The transfer of momentum between the atmosphere and ocean is usually
³ parameterised as a stress applied at the surface. Arguments originating from
⁴ the theory of vertical turbulent transfers give rise to the following expression
⁵ for the applied stress

$$\tau_{relative} = \rho_a c_d |\mathbf{U}_{10} - \mathbf{u}_s| (\mathbf{U}_{10} - \mathbf{u}_s), \quad (1)$$

⁶ where $\mathbf{U}_{10} = (U_{10}, V_{10})$ is the 10m (atmospheric) wind velocity, $\mathbf{u}_s = (u_s, v_s)$
⁷ is the surface ocean velocity, ρ_a is air density, and c_d is a drag coefficient,
⁸ which itself may be a weak function of $\mathbf{U}_{10} - \mathbf{u}_s$. We will refer to the use of
⁹ Eq. (1) to calculate wind stress as using “relative wind stress.” In the limit
¹⁰ that $\mathbf{u}_s \ll \mathbf{U}_{10}$, known as the resting ocean approximation, Eq. (1) can be
¹¹ simplified to

$$\tau_{resting} = \rho_a c_d |\mathbf{U}_{10}| \mathbf{U}_{10}. \quad (2)$$

¹² The use of relative wind stress leads to a slight decrease in the stress felt
¹³ by the ocean, relative to the resting ocean approximation. This contributes
¹⁴ to a reduction of the power input to the ocean circulation by $\sim 20 - 35\%$
¹⁵ (Duhaut and Straub, 2006; Zhai and Greatbatch, 2007; Hughes and Wilson,
¹⁶ 2008; Zhai et al., 2012). Since the power input from the wind is a major source

19 of energy to the ocean (Wunsch and Ferrari, 2004; Ferrari and Wunsch, 2009)
20 this could have significant consequences for the large-scale ocean circulation,
21 its variability, and its sensitivity to changes in surface wind stress.

22 Relative wind stress exerts a torque on individual eddies that opposes
23 their circulation and so directly damps them. This is due to the increase in
24 the velocity *difference* between ocean and atmosphere from one side of the
25 eddy to the other (see Fig. 1 of Zhai et al., 2012). This acts as a drag at
26 the surface of the ocean and significantly increases the rate of spindown of
27 waves and eddies via the introduction of “top friction” (Dewar and Flierl,
28 1987). In regions in which mesoscale eddies play an important role in ocean
29 circulation/dynamics, such as the Southern Ocean, this could indicate an
30 important role for relative wind stress.

31 The Southern Ocean is subject to strong atmospheric winds and makes a
32 large regional contribution to the global integral of mechanical power input
33 to the ocean (Wunsch, 1998). It has a strong influence on global climate, via
34 its Residual Meridional Overturning Circulation (RMOC) and the Antarctic
35 Circumpolar Current (ACC) (Meredith et al., 2011). Mesoscale eddies play
36 prominent roles in the momentum (Munk and Palmén, 1951; Johnson and
37 Bryden, 1989), heat (Bryden, 1979; Jayne and Marotzke, 2002; Meijers et al.,
38 2007), and kinetic energy (Cessi et al., 2006; Cessi, 2008; Abernathey et al.,
39 2011) budgets of the Southern Ocean. The role that relative wind stress
40 might play in the dynamics and circulation of the Southern Ocean can be
41 usefully framed in terms of a residual mean treatment of the RMOC.

42 In residual mean theory, the streamfunction of the RMOC is written as
43 the combination of the Eulerian mean MOC ($\bar{\Psi}$) and the eddy-induced bolus

44 overturning (Ψ^*) (see, e.g., Marshall and Radko, 2003), i.e.

45

$$\Psi_{\text{res}} = \bar{\Psi} + \Psi^* = -\frac{\bar{\tau}_x}{\rho_0 f} + Ks. \quad (3)$$

46 In Eq. (3), $\bar{\tau}_x$ is the time-mean zonal wind stress, ρ_0 is the Boussinesq
47 reference density, f is the Coriolis parameter, K is the quasi-Stokes/eddy
48 diffusivity for the buoyancy field ($b = -g(\rho - \rho_0)/\rho_0$) and $s = -\bar{b}_y/\bar{b}_z$ is the
49 isopycnal slope. There are a considerable number of ways to formulate the
50 dependence of K on external parameters. For the current purpose, the most
51 informative is to use mixing length theory (Prandtl, 1925) to relate K to
52 the product of an eddy length and eddy velocity scale, i.e. L_{eddy} and U_{eddy} ,
53 such that $K = L_{\text{eddy}}U_{\text{eddy}}$ (see, e.g., Green, 1970; Stone, 1972; Eden and
54 Greatbatch, 2008).

55 In Eq. (3), it is the mean wind stress that plays a role in setting the
56 residual overturning. Relative wind stress can therefore directly impact the
57 residual overturning by reducing $\bar{\tau}_x$. Furthermore, the direct damping of the
58 eddy field can be reasonably expected to alter both L_{eddy} and U_{eddy} , i.e. K ,
59 and, hence, the eddy-induced bolus overturning and net RMOC. Intuition
60 suggests that damping the eddy field will reduce U_{eddy} and K , and hence Ψ^* .

61 A further indirect effect can also occur through the isopycnal slope, s ,
62 which can be related to the zonal volume transport of the ACC via thermal
63 wind. Eddies play a large role in setting the stratification of the ocean (e.g.
64 Karsten et al., 2002) as part of a dynamic balance with other processes.
65 Damping eddies at the surface may alter the balance between processes that
66 set the stratification and so change s . This would then have a knock-on effect
67 on the bolus overturning and zonal transport of the ACC. As an example,

68 in the quasi-geostrophic Southern Ocean simulations of Hutchinson et al.
69 (2010) the use of relative wind stress results in a 38Sv *increase* in circumpolar
70 transport. This comes about due to steepening of isopycnals and an increase
71 in the geostrophic velocity field via thermal wind shear.

72 The above discussion is framed in terms of a particular wind stress and the
73 ocean circulation/stratification that results. However, when the wind stress
74 over the Southern Ocean changes, the mesoscale eddy field also responds.
75 This leads to a decrease in the sensitivity of the circumpolar transport of
76 the ACC (Hallberg and Gnanadesikan, 2001; Tansley and Marshall, 2001)
77 and of the RMOC (Hallberg and Gnanadesikan, 2006; Farneti et al., 2010)
78 to changes in wind stress when the eddy field is resolved instead of param-
79 eterised. These phenomena are known as eddy saturation (Straub, 1993)
80 and eddy compensation (Viebahn and Eden, 2010), respectively. Although
81 there are subtleties to the degree of eddy saturation/compensation that a
82 particular model may exhibit, e.g. the presence of shallow coastal shelves
83 (Hogg and Munday, 2014) or surface breaking continents (Munday et al.,
84 2015) and the use of fixed heat/buoyancy fluxes vs. restoring to a fixed tem-
85 perature/buoyancy profile (Abernathay et al., 2011; Zhai and Munday, 2014,
86 henceforth AMF11 and ZM14, respectively), their emergence upon resolution
87 of an eddy field is robust in many respects.

88 Many of the above cited papers use idealised model configurations to
89 investigate the effect changing wind stress on circumpolar transport and/
90 or the RMOC. In doing so, they usually use a specified wind stress (e.g.
91 AMF11; ZM14; Morrison and Hogg, 2013; Munday et al., 2013). Applying
92 a constant wind stress is certainly within the idealised spirit and design of

93 such experiments. However, it rules out the direct damping of the mesoscale
94 eddy field that takes place under relative wind stress and the role that this
95 might play in setting the sensitivity of the RMOC and/or stratification to
96 changing winds.

97 In this paper we seek to answer the following questions: 1) can the impact
98 of relative wind stress be modelled simply by accounting for the reduced
99 mean wind stress? 2) does the direct damping of the mesoscale eddy field
100 have implications for Southern Ocean dynamics? 3) does relative wind stress
101 significantly alter the sensitivity of the circumpolar transport and the RMOC
102 to wind stress changes?

103 We begin in Section 2 with a brief description of the experimental design
104 and model domain. The control simulations of three suites of experiments
105 are discussed in Section 3. Section 4 briefly derives a simplified mechanical
106 energy budget for the ocean including the effects of relative wind stress.
107 The sensitivity to wind stress changes across the full suite of experiments
108 is discussed in Section 5. We close with a summary and discussion of our
109 results in Section 6.

110 [Table 1 about here.]

111 **2. Experimental Design**

112 In order to investigate the impact of relative wind stress, and its associ-
113 ated eddy damping effects, on Southern Ocean dynamics we adopt the ide-
114 alised MIT general circulation model (MITgcm, see Marshall et al., 1997a,b)
115 configuration of AMF11, adapted to a coarser grid spacing by ZM14. This
116 model domain is a zonally re-entrant channel that is 1000km in zonal extent,

117 nearly 2000km in meridional extent, and 2985m deep with a flat bottom.
 118 There are 33 geopotential levels whose thickness increase with depth, rang-
 119 ing from 10m at the surface to 250m for the bottom-most level.

120 The horizontal grid spacing is chosen to be 10km, which is sufficiently fine
 121 so as to permit a vigorous eddy field without incurring undue computational
 122 cost. This grid spacing makes the model eddy-permitting, rather than eddy-
 123 resolving, with the control wind stress (see below for forcing details) giving
 124 a first baroclinic Rossby radius in the range of ~ 5 km near the southern
 125 boundary and ~ 25 km near the northern. It is important to note that the
 126 eddies are generally several multiples of the deformation radius in size and
 127 that use of a 10km grid spacing does not preclude the emergence of a high
 128 degree of eddy saturation (Munday et al., 2015) and as such we deem it
 129 sufficient for our purposes.

130 We employ the K-profile parameterisation (KPP) vertical mixing scheme
 131 (Large et al., 1994) and a linear bottom friction in addition to the much
 132 weaker drag from a noslip bottom boundary condition. The equation of
 133 state is linear and only temperature variations are considered. The model
 134 is set on a β -plane and lateral boundaries are noslip. Parameters values for
 135 bottom friction, viscosity, etc, are as given in Table 1.

136 The model's potential temperature, θ , is forced by a heat flux at the
 137 surface given by

$$138 Q(y) = \begin{cases} -Q_0 \sin(3\pi y/L_y), & \text{for } y < L_y/3 \\ 0, & \text{for } y > L_y/3 \end{cases} \quad (4)$$

139 as per AMF11 and ZM14, except $y = 0$ km is placed at the centre of the

140 domain. This broadly describes the observed distribution of surface buoyancy
141 flux around the Southern Ocean (see Fig. 1 of AMF11). Within 100km of
142 the northern boundary, potential temperature is restored to the stratification
143 given by

144

$$\theta_N(z) = \Delta\theta \left(e^{z/h_e} - e^{-H/h_e} \right) / \left(1 - e^{-H/h_e} \right). \quad (5)$$

145 The restoring time scale for the sponge varies from ∞ (no restoring) at the
146 southern edge of the sponge to 7 days at the northern edge of the domain.
147 The surface buoyancy flux and sponge restoring profile are as shown in Figs.
148 1a and 1b.

149 [Figure 1 about here.]

150 In contrast to AMF11 and ZM14, we do not prescribe the wind stress
151 in the majority of our experiments. Instead we prescribe wind velocity and
152 use the bulk formulae of Large and Pond (1981), i.e. Eqs. (1) and (2), to
153 calculate the wind stress. The wind velocity is given by

154

$$\mathbf{U}_{10} = \mathbf{U}_0 \cos(\pi y/L_y), \quad (6)$$

155 where $\mathbf{U}_0 = (U_x, U_y)$ is the peak wind velocity in the zonal and meridional
156 direction. For the experiments considered here, the peak meridional wind,
157 U_y , is set to zero and the peak zonal wind, U_x , varies from 0m s^{-1} to 20m s^{-1} .
158 Representative examples of the zonal wind that arises from Eq. (6) are shown
159 in Fig. 1c.

160 In total, we have performed 3 sets of 8 experiments. The first 8 of these
161 we refer to as the resting ocean experiments. These use peak zonal wind

162 velocities of 0, 3, 7, 10, 12, 16, 18, and 20ms^{-1} with the resultant wind
163 stress calculated as per Eq. (2). There is no meridional wind, and thus no
164 meridional wind stress, in these experiments. The wind stresses that zonal
165 wind velocities of 3, 12, and 20ms^{-1} produce are shown in Fig. 1d.

166 We refer to the second set of 8 experiments as the relative wind stress
167 experiments. These use the same peak zonal wind velocities as the resting
168 ocean experiments, but Eq. (1) is used to calculate the wind stress. This gives
169 a slight decrease in the peak zonal wind stress and introduces a very weak
170 (absolute magnitude $\lesssim 0.05\text{N m}^{-2}$ when $U_x = 20\text{ms}^{-1}$) meridional stress.

171 For the final set of 8 experiments, we use a 50 year average of the zonal
172 and meridional wind stress from the relative wind stress experiments to drive
173 the ocean. This includes the very weak meridional stress. We refer to these
174 as the equivalent wind stress experiments.

175 The resting ocean and relative wind stress experiments are begun from
176 the statistically steady control experiment of ZM14 with the wind stress
177 replaced with the wind velocities described above. They are run to their
178 new statistical steady state. At the end of this phase of spin up we perform
179 a 50 year diagnostic run, from which all subsequent figures and conclusions
180 are drawn. The 50 year average of the zonal and meridional wind stress
181 diagnosed from this time period are then used to drive the equivalent wind
182 stress experiments. These are run to their statistical steady state, after which
183 an additional 50 year diagnostic run is carried out.

184 **3. The Control State**

185 *3.1. Zonal Circulation of the Control State*

186 For our control experiments we select a peak zonal wind speed of 12 m s^{-1} .
187 This gives a peak zonal wind stress of 0.208 N m^{-2} for the relative wind stress
188 and equivalent wind stress experiments, very close to the control wind stress
189 used by AMF11 and ZM14 (0.2 N m^{-2}). The peak zonal wind stress is slightly
190 higher for the resting ocean experiments at 0.222 N m^{-2} . Due to the flat
191 bottom, the time-average circulation of all of our experiments is very close
192 to zonally symmetric with mean streamlines closely aligned with contours of
193 potential temperature (not shown).

194 Assuming a purely zonal time-mean wind stress, since $\bar{\tau}_y \ll \bar{\tau}_x$ for all
195 of the relative and equivalent wind stress experiments, the depth-integrated
196 zonal momentum budget of a flat bottomed channel is approximately (see,
197 e.g. Gill and Bryan, 1971)

$$198 \quad \frac{\langle \bar{\tau}_x \rangle}{\rho_0} \approx r_b \langle \bar{u}_b \rangle, \quad (7)$$

199 where the overbar indicates a time average, the angled braces an average in
200 the zonal direction and the subscript b indicates the bottom value. This ap-
201 proximate budget indicates that the bottom flow accelerates until the linear
202 bottom friction can balance the momentum source at the surface. This leads
203 to large zonal transport in models without bathymetry.

204 [Table 2 about here.]

205 On the basis of Eq. (7), the total circumpolar transport of the mean
206 zonal flow (T_{ACC}) can be decomposed into contributions due to changes in

207 the bottom flow and that due to changes in thermal wind shear (see Munday
208 et al., 2015, for details). We refer to the depth and zonal integral of $\langle \bar{u}_b \rangle$ as
209 the “bottom transport” (T_b) and the difference between this and the total
210 transport as the “thermal wind transport”, given by $T_{tw} = T_{ACC} - T_b$.

211 For the relative and equivalent wind stress control experiments, there is
212 no difference in T_b (see Table 2), as one would expect from Eq. (7). In the
213 resting ocean control, the wind stress is increased and so, therefore, is the
214 resulting T_b . The increase in T_b due to higher wind stress dominates the
215 change in T_{ACC} between the resting ocean control experiment and the other
216 two controls. In contrast, for T_{tw} the relative wind stress and resting ocean
217 controls both show a 1 Sv increase with respect to the equivalent wind stress
218 control. This is due to changes in isopycnal slope and the buoyancy change
219 across the current (see Section 3.3 for further discussion).

220 *3.2. Residual Overturning of the Control State*

221 [Figure 2 about here.]

222 Following AMF11 and ZM14, the model’s RMOC is diagnosed using po-
223 tential temperature as the vertical coordinate. The calculations uses discrete
224 layers that are 0.2°C thick and is interpolated back to depth coordinates on
225 the model’s geopotential layers. The eddy-induced bolus overturning, Ψ^* ,
226 can then be calculated using $\Psi^* = \Psi_{res} - \bar{\Psi}$, where $\bar{\Psi}$ is the Eulerian mean
227 overturning.

228 The RMOC of all three control experiments closely resembles that of
229 the control experiments of AMF11 and ZM14, as shown in Fig. 2. The
230 Eulerian overturning is very similar for the relative wind stress and equivalent

231 wind stress cases (not shown). Therefore, any significant difference between
232 these two experiments arises through modification of the eddy-induced bolus
233 overturning. The resting ocean experiment with the same wind speed has a
234 slightly more intense Eulerian overturning due to the 7% increase in $\langle \bar{\tau}_x \rangle$.

235 In general, the differences between the control RMOCs in Figs. 2 are
236 relatively minor. The upwelling North Atlantic Deep Water (NADW) cell
237 (red) and the downwelling Antarctic Bottom Water (AABW) cell (blue, near
238 the southern boundary) are all broadly the same strength and at roughly the
239 same depth/temperature range. To quantify the strength of the cells, we use
240 the same method as AMF11 and select the maximum and minimum value of
241 Ψ_{res} below 500m and 100km south of the edge of the sponge region. These
242 values are labeled Ψ_{upper} and Ψ_{lower} for the NADW and AABW cells, respec-
243 tively. For the three control experiments, the strength of the NADW and
244 AABW cells are very similar at depth (see Table 2). This implies that there
245 has not been a large-scale weakening of the eddy-induced bolus overturn-
246 ing due to the damping of the eddy field in the relative wind stress control
247 experiment.

248 Examination of the mixed layer, defined as above the depth at which the
249 water is 0.8°C colder than the surface (above the grey line in Fig. 2, see,
250 e.g., Kara et al., 2000, for details), indicates that this is the region where
251 the biggest differences between the control experiments occur. To quantify
252 the strength of the RMOC in the mixed layer we select the maximum value
253 above 500m and the minimum value above 500m, and within the southern
254 half of the domain (to ensure selecting a value from the AABW cell). These
255 measures are labeled $\Psi_{\text{m+}}$ and $\Psi_{\text{m-}}$, respectively, in Table 2 and are intended

256 to highlight any large-scale changes in the flow within the mixed layer. For
257 the relative wind stress control experiment $\Psi_{m+} = 0.84\text{Sv}$ and is $\sim 30\%$
258 higher than for either of the other two control experiments. In contrast, the
259 Ψ_{m-} values are only marginally different.

260 Due to the relative and equivalent wind stress controls having the same
261 Eulerian overturning, the reduced value Ψ_{m+} for the relative control must be
262 due to a weaker eddy-induced bolus overturning within the mixed layer. The
263 NADW cell is placed under the strongest wind forcing, where the damping
264 of the eddy field by relative wind stress is also strongest. Hence, it is un-
265 surprising that the largest changes to the RMOC take place in this locale.
266 In contrast, the similar value of Ψ_{m-} for the relative and equivalent wind
267 stress experiments imply that their bolus overturning is also similar within
268 the confines of the AABW cell.

269 Close examination of Fig. 2 reveals that whilst the distribution in depth
270 coordinates is grossly the same, there are changes in the temperature distri-
271 bution of the RMOC. For example, the 0.5°C isotherm is within the AABW
272 cell for the relative wind stress control experiment. However, this isotherm
273 is lower in the water column, and thus removed from the AABW cell in the
274 other two control experiments. Within the NADW cell, which is where we
275 focus most of our attention, the differences are much smaller. Damping of
276 the eddy field alters the stratification and exposes different temperatures to
277 difference heat and momentum fluxes at the surface. Since the RMOC must
278 “match” this forcing (Walsh, 1982; Badin and Williams, 2010), it has to take
279 place at this altered temperature range.

280 3.3. Eddy Kinetic Energy and Vertical Stratification

In terms of surface Eddy Kinetic Energy (EKE), the direct damping of the eddy field by relative wind stress is far more important than the slight decrease in mean wind stress with respect to the resting ocean approximation. This is illustrated in the surface EKE maps of Fig. 3a-c. The $\sim 3\%$ decrease in surface average EKE between Figs. 3b and 3c is caused by the 7% reduction in mean wind stress between the equivalent wind stress and resting ocean control experiments. However, in Fig. 3a the surface average EKE has decreased by a further $\sim 15\%$, relative to Fig. 3b.

289 [Figure 3 about here.]

290 [Figure 4 about here.]

291 The difference in EKE between the relative and equivalent wind stress
 292 experiments persists throughout the water column, as shown in Fig. 4a.
 293 This contrasts with the effect of surface heat flux damping of EKE, which
 294 is confined to roughly the top 100m (see Fig. 5a of ZM14). The magnitude
 295 of this difference decays with depth, such that it is not a simple step change
 296 throughout the domain. In contrast, temperature variance shows only a
 297 slight difference at mid-depths, with the surface and bottom values being
 298 very similar between the relative and equivalent wind stress experiments
 299 (see Fig. 4b).

In Fig. 5 it is noteworthy that the isotherms in the relative wind stress control (red lines) are nearly always steeper than the isotherms of the equivalent wind stress control (blue lines). Furthermore, they are also quite often steeper than the isotherms of the resting ocean control (green line), despite

304 the weaker wind stress. This can be attributed to the surface eddy damping
305 from relative wind stress, which has led to a change in the balance between
306 the mean flow and eddies that sets the stratification.

307 The effect that reduced EKE under relative wind stress might have can
308 be illustrated with a simple thought experiment. Imagine an equilibrated
309 system is impulsively switched from resting ocean to relative wind stress
310 without changing the mean wind stress. This impulsive switch would damp
311 the EKE at the surface and also reduce the eddy heat transport. In terms of
312 the residual overturning, the reduction in EKE would decrease K and thus
313 the eddy-induced bolus overturning. Since the mean wind stress has been
314 kept constant, the Eulerian overturning will then steepen the isopycnals.
315 This steepening will be arrested when the RMOC is again in balance with
316 the surface heat fluxes.

317 [Figure 5 about here.]

318 As noted in Section 3.1, the circumpolar transport due to T_{tw} is different
319 between the relative and equivalent wind stress experiments. This is partly
320 due to the more steeply sloping isopycnals moving meridional gradients into
321 regions of lower f . Primarily, however, it is because the water at the south-
322 ern boundary tends to be less buoyant, as a result of the changes in mean
323 stratification and heat transport. This increase in T_{tw} between the relative
324 and equivalent wind stress experiments is consistent with the results and ar-
325 guments of Hutchinson et al. (2010). However, the 1Sv difference between
326 our control experiments is considerably smaller than the 38Sv between the
327 experiments of Hutchinson et al. (2010) (see Section 5.1 for further comment).

328 **4. The Mechanical Energy Budget Under Relative Wind Stress**

329 Before examining the sensitivity of key diagnostics to wind stress changes
330 under different wind stress bulk formulae, we first give a short derivation
331 of the approximate mechanical energy balance expected in a flat bottomed
332 channel. This is a restatement of the results of AMF11 taking into account
333 the extra “top friction” of Dewar and Flierl (1987).

334 In contrast to the approximate zonal momentum budget of Eq. (7), we
335 retain the meridional component of the time-varying wind stress, i.e. $\boldsymbol{\tau}' =$
336 (τ'_x, τ'_y) . Since τ'_y is a function of the eddy velocities, it is not obvious that
337 it makes a negligible contribution to the energy budget. Following Cessi
338 et al. (2006) and Cessi (2008), the leading order mechanical eddy budget is
339 expected to be

340
$$\langle \overline{\boldsymbol{\tau} \cdot \mathbf{u}_s} \rangle \approx \rho_0 r_b \langle \overline{\mathbf{u}_b \cdot \mathbf{u}_b} \rangle, \quad (8)$$

341 i.e. that surface wind power input is balanced by bottom kinetic energy
342 dissipation. After Reynolds averaging in time, this becomes

343
$$\langle \overline{\tau_x \mathbf{u}_s} \rangle + \langle \overline{\boldsymbol{\tau}' \cdot \mathbf{u}'_s} \rangle \approx \rho_0 r_b \langle \overline{\mathbf{u}_b^2} \rangle + \rho_0 r_b \langle \overline{\mathbf{u}'_b \cdot \mathbf{u}'_b} \rangle, \quad (9)$$

344 where we have used that $\overline{\tau}_y \ll \overline{\tau}_x$ and $\overline{v}_b \ll \overline{u}_b$. After AMF11, and assuming
345 only small deviations from the zonal mean, we may then use Eq. (7) to
346 rewrite this as

347
$$\langle \overline{\tau}_x (\overline{\mathbf{u}}_s - \overline{\mathbf{u}}_b) \rangle = - \langle \overline{\boldsymbol{\tau}' \cdot \mathbf{u}'_s} \rangle + \rho_0 r_b \langle \overline{\mathbf{u}'_b \cdot \mathbf{u}'_b} \rangle. \quad (10)$$

348 Following Duhaut and Straub (2006), we use that $|\mathbf{U}_{10}| \gg |\mathbf{u}_s|$ to write

349 $|\mathbf{U}_{10} - \mathbf{u}_s| \approx |\mathbf{U}_{10}| - \mathbf{u}_s \cdot \mathbf{k}$, where \mathbf{k} is a unit vector in the direction of
 350 the atmospheric wind. Assuming that the atmospheric wind is purely zonal,
 351 eastward and constant in time, this can be further simplified to $|\mathbf{U}_{10}| - \mathbf{u}_s \cdot \mathbf{k} \approx$
 352 $U_{10} - u_s$. With the additional assumption of constant c_d , Eq. (1) can be
 353 written as

$$354 \quad \boldsymbol{\tau}_{relative} \approx \rho_a c_d (U_{10} - \bar{u}_s - u'_s) (\mathbf{U}_{10} - \bar{\mathbf{u}}_s - \mathbf{u}'_s) \quad (11)$$

355 where it is important to note that $\rho_a c_d (U_{10} - \bar{u}_s - u'_s)$ is a scalar quantity
 356 and we have written the surface ocean velocity as the sum of its time-mean
 357 ($\bar{\mathbf{u}}_s$) and a small perturbation (\mathbf{u}'_s).

358 Via Reynolds' averaging, the time average wind stress can then be ap-
 359 proximated by

$$360 \quad \bar{\boldsymbol{\tau}}_{relative} \approx r_s (\mathbf{U}_{10} - \bar{\mathbf{u}}_s) + \rho_a c_d \bar{u}'_s \bar{\mathbf{u}}'_s \quad (12)$$

361 where $r_s = \rho_a c_d (U_{10} - \bar{u}_s)$. For the zonal component of the wind stress, the
 362 first term on the right-hand-side of Eq. (12), equivalent to $\rho_a c_d (U_{10} - \bar{u}_s)^2$,
 363 will always be considerably larger in magnitude than the second, $\rho_a c_d \bar{u}'_s \bar{u}'_s$,
 364 and both are positive definite. The first term then reflects the well-known
 365 reduction in wind stress, with respect to the resting ocean approximation,
 366 that relative wind stress achieves with the same wind velocity. In this case
 367 primarily because the strong zonal flow of the circumpolar flow is in the same
 368 direction as the imposed atmospheric wind.

369 For the meridional wind stress, the first term on the right-hand-side of
 370 Eq. (12) is given by $-\rho_a c_d (U_{10} - \bar{u}_s) \bar{v}_s$ and so opposes the mean flow as an
 371 additional form of “top friction” due to Dewar and Flierl (1987). The second
 372 term on the right-hand-side is $\rho_a c_d \bar{u}'_s \bar{v}'_s$, which is sign indefinite and so may

373 act to either increase or decrease the mean meridional wind stress.

374 Based on Reynolds' averaging, the time-varying wind stress perturbation
375 under relative wind stress can be approximated by

$$376 \quad \tau'_{relative} \approx -\rho_a c_d u'_s (\mathbf{U}_{10} - \bar{\mathbf{u}}_s) - r_s \mathbf{u}'_s + \rho_a c_d u'_s \mathbf{u}'_s - \rho_a c_d \bar{u}'_s \bar{\mathbf{u}}'_s, \quad (13)$$

377 which time-averages to zero. An equivalent to the expression of Duhaut and
378 Straub (2006) for the difference in power input to the ocean between the
379 resting ocean approximation and relative wind stress forcing (their Eq. (6))
380 can now be derived.

381 By taking the dot product of Eq. (13) with the time-varying velocity and
382 time-averaging, the following expression for the power input due to variations
383 of the wind stress acting on variations of the ocean current results

$$384 \quad \overline{\tau' \cdot \mathbf{u}'_s} \approx -\rho_a c_d (\mathbf{U}_{10} - \bar{\mathbf{u}}_s) \cdot \overline{u'_s \mathbf{u}'_s} - r_s \overline{\mathbf{u}'_s \cdot \mathbf{u}'_s} + \rho_a c_d \overline{u'_s \mathbf{u}'_s \cdot \mathbf{u}'_s}. \quad (14)$$

385 Assuming that $\bar{v}_s \ll \bar{u}_s$, consistent with the equivalent assumption regard-
386 ing the bottom flow in Eq. (10), and neglecting the triple correlation, this
387 becomes

$$388 \quad \overline{\tau' \cdot \mathbf{u}'_s} \approx -r_s \overline{u'_s u'_s} - r_s \overline{\mathbf{u}'_s \cdot \mathbf{u}'_s} \approx -\frac{3}{2} r_s \overline{\mathbf{u}'_s \cdot \mathbf{u}'_s}. \quad (15)$$

389 In Eq. (15), we have further assumed that $\overline{u'_s u'_s} \approx \overline{\mathbf{u}'_s \cdot \mathbf{u}'_s}/2$, following the
390 argument of Hughes and Wilson (2008). This is effectively a statement that
391 eddies are close to circular in shape. Whilst this is not strictly the case in a
392 realistic domain with complex bathymetry, it is a reasonably good approxi-
393 mation in our zonally-symmetric channel domain.

394 This allows Eq. (10) to be written as

395
$$\langle \bar{\tau}_x (\bar{u}_s - \bar{u}_b) \rangle = \frac{3}{2} r_s \langle \bar{\mathbf{u}}'_s \cdot \bar{\mathbf{u}}'_s \rangle + \rho_0 r_b \langle \bar{\mathbf{u}}'_b \cdot \bar{\mathbf{u}}'_b \rangle. \quad (16)$$

396 As the surface wind speed increases, Eq. (16) indicates an increase in the
397 available power to drive the mesoscale eddy field, as per AMF11. However,
398 some of the extra power input goes into overcoming the additional dissipation
399 due to relative wind stress, characterised by the additional term with respect
400 to Eq. (25) of AMF11.

401 The magnitude of the extra term can be assessed via scaling. The surface
402 EKE is roughly an order of magnitude bigger than the bottom EKE (see Fig.
403 4). Taking into account the coefficients of the two terms, i.e. $\rho_0 r_b \sim 1$ and
404 $r_s = \rho_a c_d (U_{10} - \bar{u}_s) \sim 0.01$, the first term on the right-hand-side of Eq. (16)
405 is roughly 15% of the second term.

406 **5. Sensitivity to Wind Speed Changes**

407 *5.1. Momentum and Energy Diagnostics*

408 [Figure 6 about here.]

409 As the mean wind speed increases, so too does the mean wind stress
410 felt by the ocean (see Figs. 1c and 1d) and thus the power input to the
411 mechanical energy budget, as per Section 4. This change in power input
412 with wind stress is shown in Fig. 6a. Under the resting ocean approximation,
413 the power input is always greater than when using relative wind stress with
414 the same atmospheric wind profile. However, the difference in power input
415 between relative and equivalent wind stress experiments is very small, \sim

416 0.002–0.006PW. This is surprising given the ~ 20 –35% difference in power
417 input between resting ocean and relative wind stress formulations previously
418 reported in the literature (see Section 1). However, in this case the relevant
419 comparison is between resting ocean and relative wind stress experiments.
420 The difference between these two sets of experiments is typically ~ 10 –20%.

421 Table 2 tells us that T_{tw} is slightly higher for relative wind stress than
422 for equivalent wind stress. This means that whilst the total power input is
423 the same for pairs of relative and equivalent wind stress experiments with
424 the same wind stress (see Fig. 6a), the left-hand-side of Eq. (16) is slightly
425 higher for relative wind stress. Potentially, there is a slightly larger source
426 of mechanical energy to drive eddying motions under relative wind stress.
427 This contradicts our intuition that relative wind stress should damp eddies.
428 However, as Fig. 6b shows, the bottom EKE under relative wind stress is
429 only marginally smaller than in the equivalent wind stress experiments.

430 In contrast to bottom EKE, the surface EKE of the relative wind stress
431 experiments departs from the line occupied by the other two sets of experi-
432 ments. This indicates that the increase in wind stress between the relative
433 wind stress experiments, which is expected to increase EKE everywhere, is
434 more than offset by the increased damping at the surface.

435 An increased wind stress can lead to an increase in the circumpolar trans-
436 port by increasing $\langle u_b \rangle$, and thus T_b , and/or by steepening isopycnals and
437 changing the buoyancy difference across the channel, and thus altering T_{tw} .
438 The increase in $\langle u_b \rangle$ leads to a linear increase in T_b with wind stress, as one
439 would expect from Eq. (7) (not shown). In contrast, T_{tw} varies non-linearly
440 with wind stress, as shown in Fig. 6c.

441 At zero wind stress, the isopycnals are very close to horizontal and $T_{tw} \sim$
442 0Sv. As the wind stress begins to increase ($\langle \bar{\tau}_x \rangle \leq 0.25 \text{Nm}^{-2}$), the isopycnals
443 begin to tilt and T_{tw} increases quasi-linearly with wind. At these low wind
444 stresses, the additional friction due to relative wind stress is very low. At
445 wind stresses $> 0.25 \text{Nm}^{-2}$, the relative wind stress experiments begin to
446 depart from the line inhabited by the equivalent wind stress and resting
447 ocean experiments. The increasing “top friction” leads to slightly steeper
448 isopycnals and slightly colder water at the southern boundary. Hence, the
449 buoyancy jump across the channel is always slightly bigger than for equivalent
450 wind stress and resting ocean and a stronger transport results.

451 This sensitivity of T_{tw} to changing wind stress is consistent with the re-
452 sults of Hutchinson et al. (2010), although at a wider range of wind stresses
453 and in a primitive equation model. Most importantly, Fig. 6c indicates that
454 eddy saturation, i.e. a loss of sensitivity to changing wind stress of circumpo-
455 lar transport, will continue to take place under relative wind stress. However,
456 the maximum circumpolar transport in a completely saturated current might
457 be higher than under the resting ocean approximation.

458 *5.2. Sensitivity to Wind Stress of the RMOC*

459 [Figure 7 about here.]

460 Using the definition of Ψ_{upper} and Ψ_{lower} given in Section 3.2, Fig. 7a
461 compares the sensitivity of the NADW and AABW cells to the changing wind
462 stress across all of three sets of experiments. It is immediately apparent that
463 there is very little difference in sensitivity across the range of forcing used.
464 At high wind stress, $\bar{\tau}_x > 0.5 \text{Nm}^{-2}$, the relative wind stress experiments

465 show a marginal decrease in sensitivity. However, on balance, it would seem
 466 reasonable to conclude that the use of relative wind stress does little to alter
 467 the sensitivity of the deep RMOC to changing wind.

468 Fig. 7b uses the definition of Ψ_{m+} and Ψ_{m-} given in Section 3.2 to assess
 469 the sensitivity of the mixed layer overturning to change in wind stress. De-
 470 spite there being quite a large difference between the values of Ψ_{m+} for the
 471 control experiments, there is little obvious pattern to the differences in sensi-
 472 tivity between the three sets of experiments. This also remains true for Ψ_{m-} .
 473 The relative wind stress experiments tend towards lower absolute values for
 474 both Ψ_{m+} and Ψ_{m-} . However, this change is outside the climatological range
 475 of Southern Ocean wind stress. Therefore, it seems reasonable to conclude
 476 that the use of relative wind stress does little to alter the sensitivity of the
 477 mixed layer RMOC to changing wind stress.

478 The changes in the RMOC within the 3 sets of experiments can be un-
 479 derstood in a residual mean framework using small perturbations from a
 480 control. Typically the perturbation might be brought about by a change
 481 in wind stress. However, more generally it may be any parameter or forc-
 482 ing that influences the system. We will consider the perturbation as being
 483 between the relative and equivalent wind stress experiments with the same
 484 mean wind stressss.

485 Beginning with Eq. (3) we take small perturbations and neglect terms
 486 that are quadratic, or higher, in perturbation quantities, this gives

$$487 \Delta\Psi_{\text{res}} \approx -\frac{\Delta\bar{\tau}_x}{\rho_0 f} + \Delta K s_0 + K_0 \Delta s, \quad (17)$$

488 where K_0 and s_0 are the eddy diffusivity and isopycnal slope of a chosen

489 relative wind stress experiment. Dividing by $\Psi_0^* = K_0 s_0$, the unperturbed
 490 bolus overturning, and writing $\Delta\bar{\Psi} = -\Delta\bar{\tau}_x/\rho_0 f$, the change in the residual
 491 overturning as a fraction of the original bolus overturning is related to the
 492 fractional changes in eddy diffusivity and isopycnal slope, such that

$$493 \quad \frac{\Delta\Psi_{\text{res}}}{\Psi_0^*} \approx \frac{\Delta\bar{\Psi}}{\Psi_0^*} + \frac{\Delta K}{K_0} + \frac{\Delta s}{s_0}. \quad (18)$$

494 This relationship will be used below to quantify the role of relative wind
 495 stress in setting the sensitivity of the RMOC to changes in wind stress.

496 Fig. 7 indicates that between pairs of relative wind stress and equivalent
 497 wind stress experiments, $\Delta\Psi_{\text{res}} \approx 0$. By design, $\Delta\bar{\Psi}$ is also zero between
 498 these matched pairs of experiments. Hence, Eq. (18) reduces to

$$499 \quad \frac{\Delta s}{s_0} \approx -\frac{\Delta K}{K_0} \quad (19)$$

500 In this case, the damping of the eddy field by “top friction” reduces K and
 501 leads to an increase in s just sufficient to prevent any change in Ψ_{res} . The
 502 marginal differences seen between the three sets of experiments in Fig. 7 is
 503 then due to the quadratic terms that were neglected in Eqs. (17) and (18).

504 [Figure 8 about here.]

505 To test the relationship between Δs and ΔK we first diagnose the mean
 506 eddy diffusivity in each of our experiments using a simple flux gradient clo-
 507 sure, i.e.

$$508 \quad \langle v'\theta' \rangle = -K \left\langle \frac{\partial \bar{\theta}}{\partial y} \right\rangle. \quad (20)$$

509 The eddy diffusivity and isopycnal slope are then averaged over the central
510 100km of the channel between depths of 500m and 1500m. Perturbations are
511 taken between pairs of relative wind stress and equivalent wind stress/resting
512 ocean experiments with the same mean wind speed. This produces Fig. 8a.
513 As expected, the difference between equivalent and relative wind stress pairs
514 produces a set of points (blue dots) that lie close to, or on, the one-to-one
515 line. In contrast, the difference between resting ocean and relative wind
516 stress pairs produces a set of points (green dots) that deviate significantly
517 from this line.

518 Agreement with the simple relationship of Eq. (18) is not the sole preserve
519 of a comparison between equivalent and relative wind stress experiments in
520 which the residual and Eulerian overturning do not change. The difference
521 in residual overturning between the relative and resting experiments can be
522 similarly accounted for by progressively decreasing the degree of approxi-
523 mation in the plotted quantities. In Fig. 8b the change in wind stress is
524 included on the y-axis of the graph, i.e. using Eq. (18) with the assumption
525 of no change in residual overturning by setting the left-hand-side to zero.
526 This improves, but does not eliminate, the scatter in the green points. When
527 the change in Ψ_{res} is accounted for on the y-axis of Fig. 8c, much of the
528 remaining scatter is removed and the comparison between the resting ocean
529 and relative experiments also falls on the one-to-one line.

530 6. Discussion and Conclusions

531 The Southern Ocean plays a major role in determining the prevailing
532 climate of the Earth system. As a result, the dynamics that govern its circu-

533 lation, and the sensitivity of that circulation to forcing changes, are of great
534 interest. Since mesoscale eddies are a crucial aspect of the circulation, the
535 use of eddy-resolving numerical models has prevailed in understanding the
536 Southern Ocean. These eddy-resolving models indicate a distinct decrease in
537 sensitivity of the circumpolar transport (eddy saturation) and/or the merid-
538 ional overturning (eddy compensation) to changes in wind stress. Depending
539 on the details of the bulk formula used to calculate the stress on the ocean
540 from the atmospheric wind, i.e. relative wind stress vs. resting ocean, it
541 is possible to introduce an additional form of friction. This “top friction”,
542 due to Dewar and Flierl (1987), could have important consequences for the
543 emergence of eddy saturation and eddy compensation by directly damping
544 the eddy field at the surface of the ocean.

545 Experiments with a vigorously eddying ocean model show that the damp-
546 ing effect of relative wind stress is more important in setting the surface
547 properties of the ocean than the $\sim 7\%$ drop in mean wind stress. In particu-
548 lar, surface EKE is quite strongly reduced, whilst SST in general decreases to
549 produce slightly cooler surface waters. As pointed out by Pacanowski (1987),
550 the alteration of SST could go on to effect many aspects of a coupled ocean-
551 atmosphere system. In particular, whilst the experiments analysed here use
552 a fixed flux to force SST, the actual energy balance between the ocean and
553 atmosphere has a strong restoring component (Haney, 1971). The slightly
554 colder SST produced under relative wind stress would likely produce stronger
555 surface heat fluxes. When combined with changing wind stress, this might
556 produce a positive feedback on the increased sensitivity of the RMOC (with
557 respect to pure heat flux boundary conditions, see AMF11) that is observed

558 under restoring boundary conditions (ZM14).

559 Even though relative wind stress damps the eddy field, a form of eddy
560 saturation still takes place as wind stress increases. The total circumpolar
561 transport, T_{ACC} , always increases with wind stress due to the strong con-
562 straint on the bottom flow from the zonal momentum (see Eq. (7)). However,
563 it appears that the component of this transport due to thermal wind shear,
564 T_{tw} , would level out at some finite value at very high wind stress (see Fig.
565 6c). A key detail is that the final T_{tw} would be higher than that achieved
566 under the resting ocean approximation. This is due to a combination of
567 steeper isotherms and a larger cross-channel buoyancy jump, consistent with
568 the quasi-geostrophic experiments of Hutchinson et al. (2010).

569 It would be reasonable to expect that the damping of the surface eddy field
570 may lead to an increase in the sensitivity of the RMOC to changing wind
571 stress by reducing the ability of the system to adjust to a forcing change.
572 However, there is only marginal change to the sensitivity of the overturning
573 across the three sets of experiments considered here. In fact, because the
574 generation, as well as the damping, of the ocean's eddy field is an adjustable
575 aspect of the circulation, the decrease in eddy diffusivity is almost offset by
576 the increase in isopycnal slope. The result is an RMOC that has the same
577 sensitivity as in an ocean forced using the resting ocean approximation.

578 Relative wind stress damps the eddies adiabatically, by modifying their
579 momentum rather than their heat content. If one considers the isopycnal
580 framework of Walin (1982), in which diabatic transformations between den-
581 sity classes are used to quantify the residual overturning, it is perhaps unsur-
582 prising that relative wind stress does not play a large role in the sensitivity of

583 the RMOC. This is because the surface heat fluxes are unchanged across all
584 three sets of experiments. This is a strong constraint upon the RMOC and
585 it is only small changes in the diabatic fluxes in temperature that the eddies
586 themselves provide that can drive changes in the RMOC. Evidently, these
587 diabatic eddy fluxes, and their sensitivity to wind stress, are only slightly
588 altered under relative wind stress. This contrasts with the results of ZM14,
589 where the damping of the eddy field by strong surface restoring of the tem-
590 perature field modifies surface water mass properties diabatically. This alters
591 the heat content of individual eddies directly and, as a result, this form of
592 eddy damping is capable of changing the sensitivity of RMOC to wind stress
593 changes.

594 Our experiments use a flat bottomed ocean in order to allow direct com-
595 parisons with the results of AMF11 and ZM14. The presence of bathymetry
596 and continental obstacles can alter the circulation in a number of ways. In
597 particular, bathymetry and continents concentrate EKE behind them (see,
598 e.g., Munday et al., 2015) via modification of the channel’s instability from
599 a global to a localised form (Abernathay and Cessi, 2014). This would also
600 focus the damping effect of using relative wind stress to these same regions,
601 which may lead to a stronger suppression of the eddy field. Potentially, this
602 could give rise to a stronger role for relative wind stress in setting the degree
603 of eddy saturation/compensation in an ocean with complex bathymetry.

604 Bathymetry can block geostrophic contours and reduce the bottom flow
605 to almost zero. This eliminates the contribution that these currents make
606 to zonal transport and power input. This may lead to a larger difference in
607 the power input between experiments conducted with the resting ocean and

608 relative wind stress experiments than that seen here. Blocking of geostrophic
609 contours also leads to the generation of barotropic gyres. This may influence
610 the response of the circumpolar transport to changes in wind forcing (Nadeau
611 and Ferrari, 2015), as can the presence of gyres circulation to the north of a
612 reentrant channel (Nadeau and Straub, 2009, 2012).

613 At the 10km grid spacing used here, the eddy field is permitted, rather
614 than strictly resolved. At this grid spacing the mature eddies are typically
615 quite well represented, although their formation processes certainly are not.
616 However, as noted in Section 2, this does not prevent a high degree of eddy
617 saturation from emerging (Munday et al., 2015). Our key finding is that the
618 use of relative wind stress results in no change in sensitivity to wind stress
619 changes in the RMOC and the transport due to thermal wind shear still satu-
620 rates. Therefore, whilst using a strictly eddy-resolving model may produce a
621 different slope in Fig. 7, it is likely that the lack of a change in this slope be-
622 tween equivalent and relative wind stress experiments would remain robust.
623 Furthermore, whilst a higher resolution model, or one with bathymetry, may
624 produce a different saturated thermal wind transport, the important point
625 is that this component of the transport still becomes invariant to further
626 change at a finite wind stress.

627 Relative wind stress seems to be most important in setting the mixed
628 layer properties, such as EKE and SST. As noted above, this will alter surface
629 flux of heat and could go on to alter the uptake or release of, for example,
630 dissolved inorganic carbon. In particular, the cooling effect of relative wind
631 stress on SST increases with the wind stress and this may enhance the flux
632 of carbon into the ocean. As the Southern Ocean is an important sink of

633 anthropogenic carbon, with the future evolution of this sink being subject to
634 debate (Le Quéré et al., 2007; Law et al., 2008; Zickfeld et al., 2008; Le Quéré
635 et al., 2008), the role of relative wind stress in setting/modifying the carbon
636 flux is of interest. The Ekman transport of carbon and nutrients out of the
637 Southern Ocean feeds productivity to the north (Williams and Follows, 1998)
638 in the form of nutrient streams (Williams et al., 2006, 2011), which may also
639 enhance the role of relative wind stress in the carbon cycle.

640 **Acknowledgements**

641 DRM was supported by the British Antarctic Survey Polar Science for
642 Planet Earth Programme. Much of this work took place whilst DRM was a
643 PDRA in the Department of Physics at the University of Oxford and was sup-
644 ported by the UK Natural Environment Research Council. This work used
645 the ARCHER UK National Supercomputing Service (<http://www.archer.ac.uk>).
646 Model output is available from DRM upon request. The authors gratefully
647 acknowledge the contributions of two anonymous reviewers whose comments
648 improved the presentation and content of the paper.

649 Abernathey, R., Cessi, P., 2014. Topographic enhancement of eddy ef-
650 ficiency in baroclinic equilibration. *J. Phys. Oceanogr.* 44, 2107–2126,
651 doi:10.1175/JPO-D-14-0014.1.

652 Abernathey, R., Marshall, J., Ferreira, D., 2011. The dependence of Southern
653 Ocean meridional overturning on wind stress. *J. Phys. Oceanogr.* 41, 2261–
654 2278.

655 Badin, G., Williams, R. G., 2010. On the buoyancy forcing and residual
656 circulation in the Southern Ocean: The feedback from Ekman and eddy
657 transfer. *J. Phys. Oceanogr.* 40, 295–310.

658 Bryden, H. L., 1979. Poleward heat flux and conversion of available potential
659 energy in Drake Passage. *J. Mar. Res.* 37, 1–22.

660 Cessi, P., 2008. An energy-constrained parameterization of eddy buoyancy
661 flux. *J. Phys. Oceanogr.* 38, 1807–1820.

662 Cessi, P., Young, W. R., Polton, J. A., 2006. Control of large-scale heat
663 transport by small-scale mixing. *J. Phys. Oceanogr.* 36, 1877–1894.

664 Dewar, W. K., Flierl, G. R., 1987. Some effects of the wind on rings. *J. Phys.*
665 *Oceanogr.* 17, 1653–1667.

666 Duhaud, T. H. A., Straub, D. N., 2006. Wind stress dependence on ocean
667 surface velocity: Implications for mechanical energy input to ocean circu-
668 lation. *J. Phys. Oceanogr.* 36, 202–211.

669 Eden, C., Greatbatch, R. J., 2008. Towards a mesoscale eddy closure. *Ocean*
670 *Modell.* 20, 223–239.

671 Farneti, R., Delworth, T. L., Rosati, A. J., Griffies, S. M., Zeng, F.,
672 2010. The role of mesoscale eddies in the rectification of the Southern
673 Ocean response to climate change. *J. Phys. Oceanogr.* 40, 1539–1557,
674 doi:10.1175/2010JPO4353.1.

675 Ferrari, R., Wunsch, C., 2009. Ocean circulation kinetic energy: Reser-

676 voirs, sources, and sinks. *Annu. Rev. Fluid Mech.* 41, 253–282,
677 doi:10.1146/annurev.fluid.40.111406.102139.

678 Gill, A. E., Bryan, K., 1971. Effects of geometry on the circulation of a
679 three-dimensional southern-hemisphere ocean model. *Deep-Sea Res.* 18,
680 685–721.

681 Green, J. S., 1970. Transfer properties of the large-scale eddies and the gen-
682 eral circulation of the atmosphere. *Q. J. R. Meteorol. Soc.* 96, 157–185.

683 Hallberg, R., Gnanadesikan, A., 2001. An exploration of the role of transient
684 eddies in determining the transport of a zonally reentrant current. *J. Phys.*
685 *Oceanogr.* 31, 3312–3330.

686 Hallberg, R., Gnanadesikan, A., 2006. The role of eddies in determining the
687 structure and response of the wind-driven southern hemisphere overturn-
688 ing: Results from the Modeling Eddies in the Southern Ocean (MESO)
689 project. *J. Phys. Oceanogr.* 36, 2232–2252.

690 Haney, R. L., 1971. Surface thermal boundary condition for ocean circulation
691 models. *J. Phys. Oceanogr.* 1, 241–248.

692 Hogg, A. M., Munday, D. R., 2014. Does the sensitivity of Southern Ocean
693 circulation depend upon bathymetric details? *Phil. Trans. R. Soc A* 372,
694 doi:10.1098/rsta.2013.0050.

695 Hughes, C. W., Wilson, C., 2008. Wind work on the geostrophic ocean cir-
696 culation: An observational study of the effect of small scales in the wind
697 stress. *J. Geophys. Res.* 113, C02016, doi:10.1029/2007JC004371.

698 Hutchinson, D. K., Hogg, A. M., Blundell, J. R., 2010. Southern Ocean
699 response to relative velocity wind stress forcing. *J. Phys. Oceanogr.* 40,
700 326–339.

701 Jayne, S. R., Marotzke, J., 2002. The oceanic eddy heat transport. *J. Phys.*
702 *Oceanogr.* 32, 3328–3345.

703 Johnson, G. C., Bryden, H. L., 1989. On the size of the Antarctic Circumpolar
704 Current. *Deep-Sea Res.* 36, 39–53.

705 Kara, A. B., Rochford, P. A., Hurlburt, H. E., 2000. An optimal defini-
706 tion for ocean mixed layer depth. *J. Geophys. Res.* 105, 16 803–16821,
707 doi:10.1029/2000JC900072.

708 Karsten, R., Jones, H., Marshall, J., 2002. The role of eddy transfer in set-
709 ting the stratification and transport of a circumpolar current. *J. Phys.*
710 *Oceanogr.* 32, 39–54.

711 Large, W. G., McWilliams, J. C., Doney, S. C., 1994. Oceanic vertical mixing:
712 A review and a model with a nonlocal boundary layer parameterization.
713 *Rev. Geophys.* 32, 363–403.

714 Large, W. G., Pond, S., 1981. Open ocean momentum flux measurements in
715 moderate to strong winds. *J. Phys. Oceanogr.* 11, 324–336.

716 Law, R. M., Matear, R. J., Francey, R. J., 2008. Comment on “Saturation of
717 the Southern Ocean CO₂ sink due to recent climate change”. *Science* 319,
718 570a.

719 Le Quéré, C., Rödenbeck, C., Buitenhuis, E. T., Conway, T. J., Langenfelds,
720 ., Gomez, A., Labuschagne, C., Ramonet, M., Nakazawa, T., Metzl, N.,
721 Gillett, N., Heimann, M., 2008. Response to comments on “Saturation of
722 the Southern Ocean CO₂ sink due to recent climate change”. *Science* 319,
723 570c.

724 Le Quéré, C., Rödenbeck, C., Buitenhuis, E. T., Conway, T. J., Langenfelds,
725 R., Gomez, A., Labuschagne, C., Ramonet, M., Nakazawa, T., Metzl, N.,
726 Gillett, N., Heimann, M., 2007. Saturation of the Southern Ocean CO₂
727 sink due to recent climate change. *Science* 316 (1735-1738), 1735–1738,
728 doi:10.1126/science.1136188.

729 Marshall, J., Adcroft, A., Hill, C., Perelman, L., Heisey, C., 1997a. A finite
730 volume, incompressible Navier-Stokes model for studies of the ocean on
731 parallel computers. *J. Geophys. Res.* 102, 5753–5766.

732 Marshall, J., Hill, C., Perelman, L., Adcroft., A., 1997b. Hydrostatic, quasi-
733 hydrostatic, and non-hydrostatic ocean modeling. *J. Geophys. Res.* 102,
734 5733–5752.

735 Marshall, J., Radko, T., 2003. Residual-mean solutions for the Antarctic
736 Circumpolar Current and its associated overturning circulation. *J. Phys.*
737 *Oceanogr.* 33, 2341–2354.

738 Meijers, A. J., Bindoff, N. L., Roberts, J. L., 2007. On the total, mean,
739 and eddy heat and freshwater transports in the southern hemisphere of a
740 $\frac{1}{8}^\circ \times \frac{1}{8}^\circ$ global ocean model. *J. Phys. Oceanogr.* 37, 277–295.

741 Meredith, M. P., Woodworth, P. L., Chereskin, T. K., Marshall, D. P., Al-
742 lison, L. C., Bigg, G. R., Donohue, K., Heywood, K. J., Hughes, C. W.,
743 Hibbert, A., Hogg, A. M., Johnson, H. L., King, B. A., Leach, H., Lenn,
744 Y., Morales-Maqueda, M. A., Munday, D. R., Naveira-Garabato, A. C.,
745 Provost, C., Sprintall, J., 2011. Sustained monitoring of the Southern
746 Ocean at Drake Passage: past achievements and future priorities. Rev.
747 Geophys. 49, RG4005, doi:10.1029/2010RG000348.

748 Morrison, A. K., Hogg, A. M., 2013. On the relationship between Southern
749 Ocean overturning and ACC transport. J. Phys. Oceanogr. 43, 140–148.

750 Munday, D. R., Johnson, H. L., Marshall, D. P., 2013. Eddy saturation of
751 equilibrated circumpolar currents. J. Phys. Oceanogr. 43, 507–532.

752 Munday, D. R., Johnson, H. L., Marshall, D. P., 2015. The role of ocean gate-
753 ways in the dynamics and sensitivity to wind stress of the early Antarctic
754 Circumpolar Current. Paleoceanography 30, doi:10.1002/2014PA002675.

755 Munk, W. H., Palmén, E., 1951. Note on the dynamics of the Antarctic
756 Circumpolar Current. Tellus 3, 53–55.

757 Nadeau, L. P., Ferrari, R., 2015. The role of closed gyres in setting the zonal
758 transport of the Antarctic Circumpolar Current. J. Phys. Oceanogr. 45,
759 1491–1509, doi:10.1175/JPO-D-14-0173.1.

760 Nadeau, L. P., Straub, D. N., 2009. Basin and channel contributions to a
761 model Antarctic Circumpolar Current. J. Phys. Oceanogr. 39, 986–1002.

762 Nadeau, L. P., Straub, D. N., 2012. Influence of wind stress, wind stress curl,

763 and bottom friction on the transport of a model Antarctic Circumpolar
764 Current. *J. Phys. Oceanogr.* 42, 207–222.

765 Pacanowski, R. C., 1987. Effect of equatorial currents on surface stress. *J.*
766 *Phys. Oceanogr.* 17, 833–838.

767 Prandtl, L., 1925. Bericht über Untersuchungen zur ausgebildeten Turbulenz.
768 *Z. Angew. Math. Mech.* 5, 136–139.

769 Stone, P. H., 1972. A simplified radiative-dynamical model for the static
770 stability of rotating atmospheres. *J. Atmos. Sci.* 29, 405–418.

771 Straub, D. N., 1993. On the transport and angular momentum balance of
772 channel models of the Antarctic Circumpolar Current. *J. Phys. Oceanogr.*
773 23, 776–782.

774 Tansley, C. E., Marshall, D. P., 2001. On the dynamics of wind-driven cir-
775 cumpolar currents. *J. Phys. Oceanogr.* 31, 3258–3273.

776 Viebahn, J., Eden, C., 2010. Towards the impact of eddies on the response
777 of the Southern Ocean to climate change. *Ocean Modell.* 34, 150–165.

778 Walin, G., 1982. On the relation between sea-surface heat flow and thermal
779 circulation in the ocean. *Tellus* 34, 187–195.

780 Williams, R. G., Follows, M. J., 1998. The Ekman transfer of nutrients and
781 maintenance of new production over the North Atlantic. *Deep-Sea Res.* 45,
782 461–489.

783 Williams, R. G., McDonagh, E., Roussenov, V. M., Torres-Valdes, S., King,
784 B., Sanders, R., Hansell, D. A., 2011. Nutrient streams in the North At-
785 lantic: Advection pathways of inorganic and dissolved organic nutrients.
786 Global Biogeochem. Cycles 25, GB4008, doi:10.1029/2010GB003853.

787 Williams, R. G., Roussenov, V., Follows, M. J., 2006. Nutrient streams
788 and their induction into the mixed layer. Global Biogeochem. Cycles 30,
789 GB1016, doi:10.1029/2005GB002586.

790 Wunsch, C., 1998. The work done by the wind on the oceanic general circu-
791 lation. J. Phys. Oceanogr. 28, 2332–2340.

792 Wunsch, C., Ferrari, R., 2004. Vertical mixing, energy, and the general cir-
793 culation of the oceans. Annu. Rev. Fluid Mech. 36, 281–314.

794 Zhai, X., Greatbatch, R. J., 2007. Wind work in a model of the northwest At-
795 lantic Ocean. Geophys. Res. Lett. 34, L04606, doi:10.1029/2006GL028907.

796 Zhai, X., Johnson, H. L., Marshall, D. P., Wunsch, C., 2012. On the wind
797 power input to the ocean general circulation. J. Phys. Oceanogr. 42, 1357–
798 1365.

799 Zhai, X., Munday, D. R., 2014. Sensitivity of Southern Ocean overturning to
800 wind stress changes: Role of surface restoring time scales. Ocean Modell.
801 84, 12–25, doi:10.1016/j.ocemod.2014.09.004.

802 Zickfeld, K., Fyfe, J. C., Eby, M., Weaver, A. J., 2008. Comment on “Sat-
803 uration of the Southern Ocean CO₂ sink due to recent climate change”.
804 Science 319, 570b.

805 **List of Figures**

806 1	Model forcing as described in the text. (a) Northern boundary	
807 temperature restoring profile, (b) surface heat flux (positive		
808 into ocean), (c) atmospheric wind profile, (d) corresponding		
809 surface wind stress under the resting ocean approximation.	39	
810 2	RMOC (Sv) for the three control experiments with $U_0 =$	
811 12m s^{-1} . Black contours are the zonal-time-average potential		
812 temperature ($^{\circ}\text{C}$) and the colours are the RMOC with red in-		
813 dicating clockwise flow. The grey contour is the mixed layer		
814 depth from the KPP parameterisation.	40	
815 3	Surface EKE (cm^2s^{-1}) for the control wind forcing with $U_0 =$	
816 12m s^{-1}	41	
817 4	Depth profiles of horizontally-averaged quantities. (a) EKE	
818 and (b) temperature variance. Medium-weight lines are the		
819 three control experiments with $U_0 = 12\text{m s}^{-1}$, thin lines have		
820 $U_0 = 0\text{m s}^{-1}$, and heavy lines have $U_0 = 20\text{m s}^{-1}$	42	
821 5	Zonally-averaged potential temperature for the three control	
822 states with $U_0 = 12\text{m s}^{-1}$. Green contours are the resting		
823 ocean control, blue contours are the equivalent wind stress		
824 control, and red contours are the relative wind stress control. .	43	
825 6	Sensitivity to wind stress changes of energy and momentum	
826 diagnostics. (a) Power input vs. maximum wind stress, (b)		
827 surface/bottom EKE vs. power input, (c) “baroclinic” trans-		
828 port, as per T_{tw} vs. maximum wind stress.	44	
829 7	Sensitivity of the RMOC to changing wind stress across all	
830 experiments. (a) Maximum/minimum RMOC 100km south		
831 of the northern restoring zone and below 500m, (b) max-		
832 imum/minimum RMOC in upper 500m (minimum also re-		
833 stricted to southern half of domain).	45	

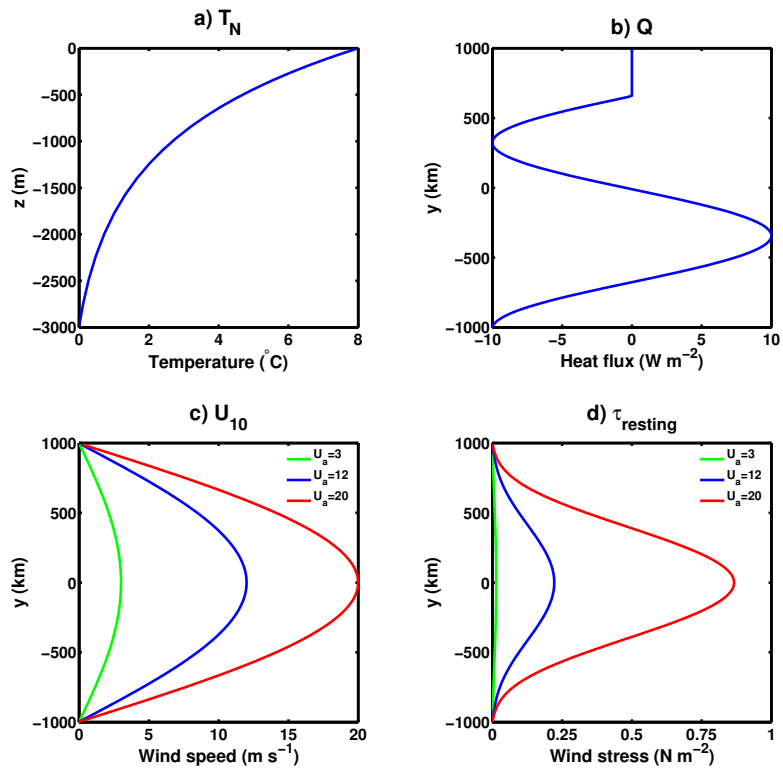


Figure 1: Model forcing as described in the text. (a) Northern boundary temperature restoring profile, (b) surface heat flux (positive into ocean), (c) atmospheric wind profile, (d) corresponding surface wind stress under the resting ocean approximation.

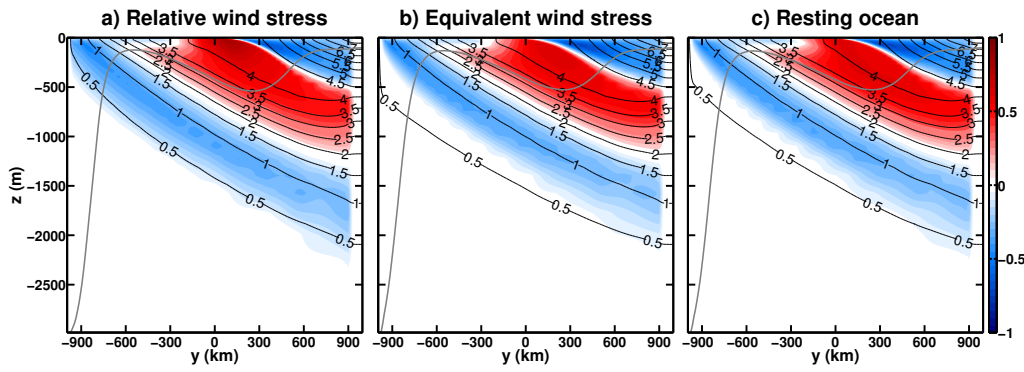


Figure 2: RMOC (Sv) for the three control experiments with $U_0 = 12\text{ m s}^{-1}$. Black contours are the zonal-time-average potential temperature ($^{\circ}\text{C}$) and the colours are the RMOC with red indicating clockwise flow. The grey contour is the mixed layer depth from the KPP parameterisation.

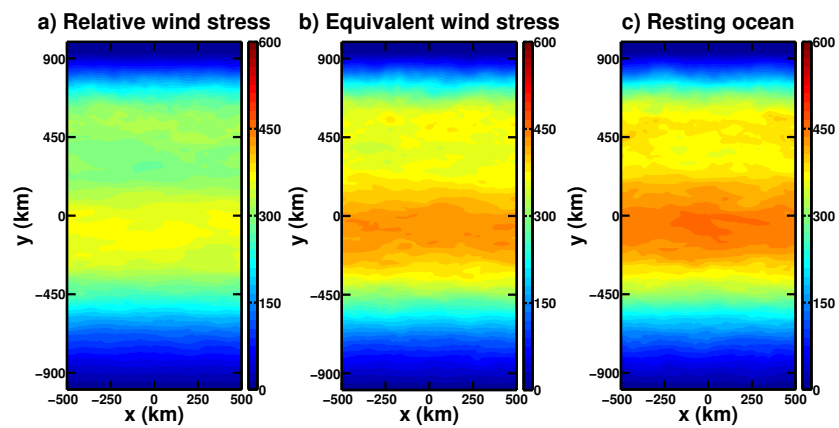


Figure 3: Surface EKE (cm²s⁻¹) for the control wind forcing with $U_0 = 12\text{m s}^{-1}$.

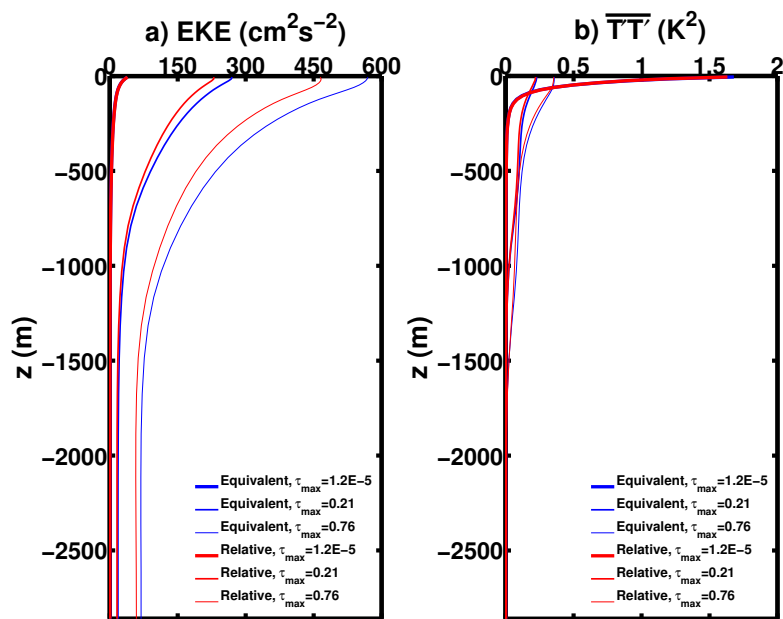


Figure 4: Depth profiles of horizontally-averaged quantities. (a) EKE and (b) temperature variance. Medium-weight lines are the three control experiments with $U_0 = 12 m s^{-1}$, thin lines have $U_0 = 0 m s^{-1}$, and heavy lines have $U_0 = 20 m s^{-1}$

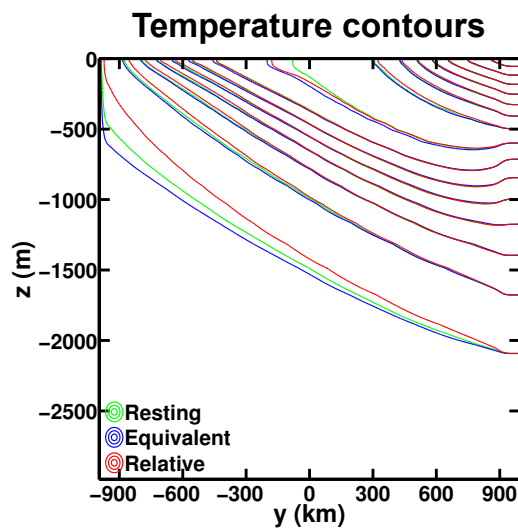


Figure 5: Zonally-averaged potential temperature for the three control states with $U_0 = 12 \text{ m s}^{-1}$. Green contours are the resting ocean control, blue contours are the equivalent wind stress control, and red contours are the relative wind stress control.

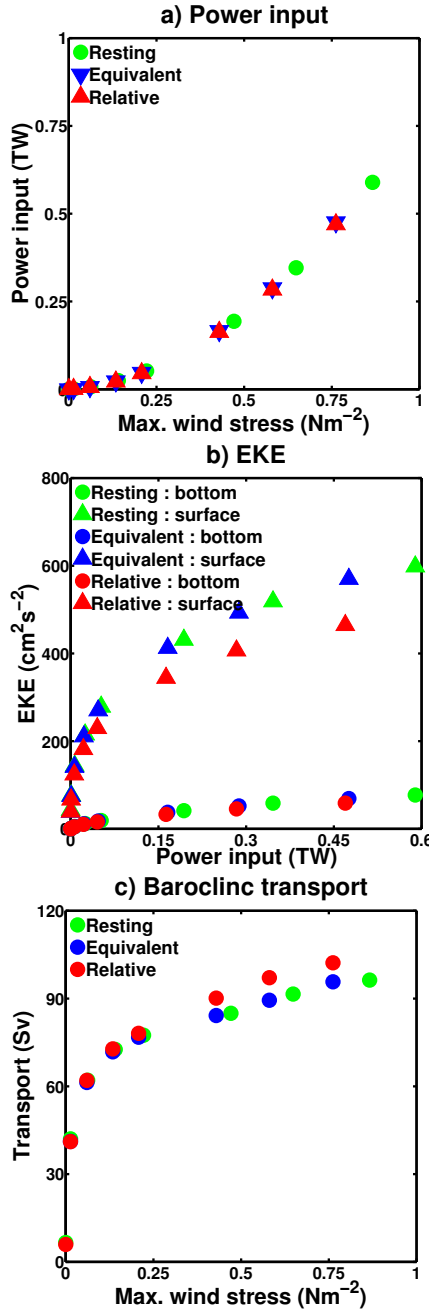


Figure 6: Sensitivity to wind stress changes of energy and momentum diagnostics. (a) Power input vs. maximum wind stress, (b) surface/bottom EKE vs. power input, (c) ‘baroclinic’ transport, as per T_{tw} vs. maximum wind stress.

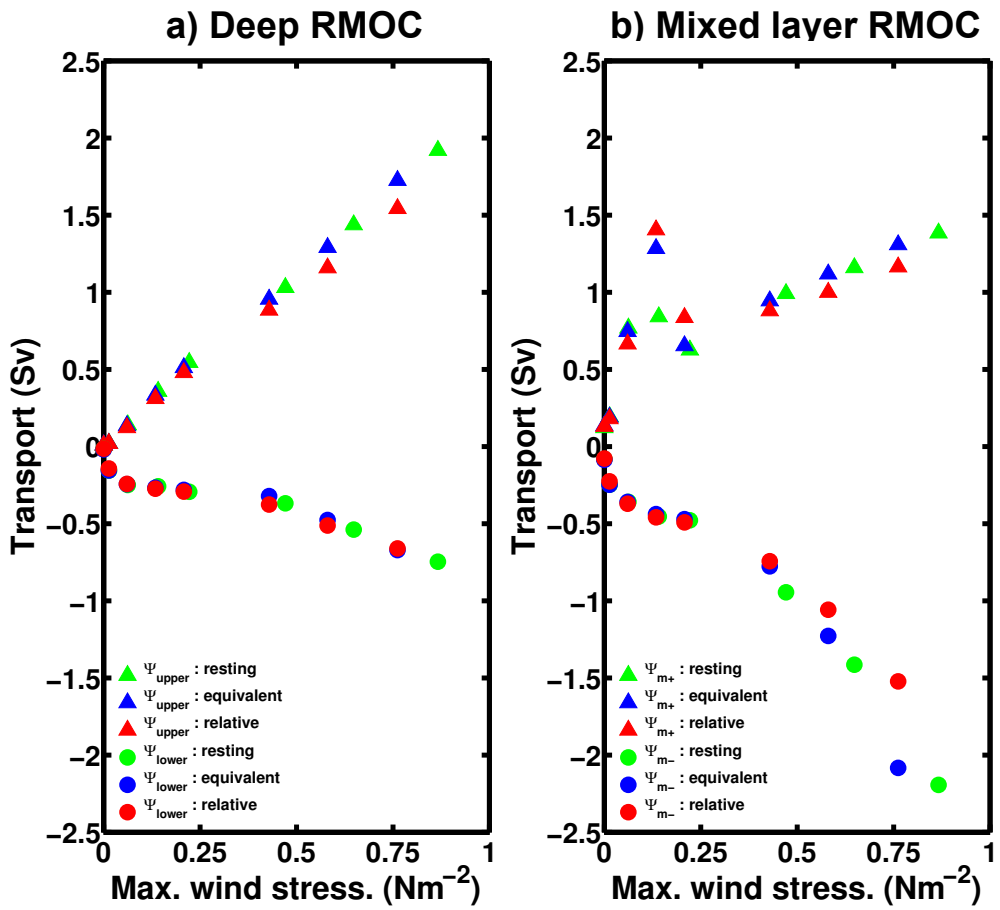


Figure 7: Sensitivity of the RMOC to changing wind stress across all experiments. (a) Maximum/minimum RMOC 100km south of the northern restoring zone and below 500m, (b) maximum/minimum RMOC in upper 500m (minimum also restricted to southern half of domain).

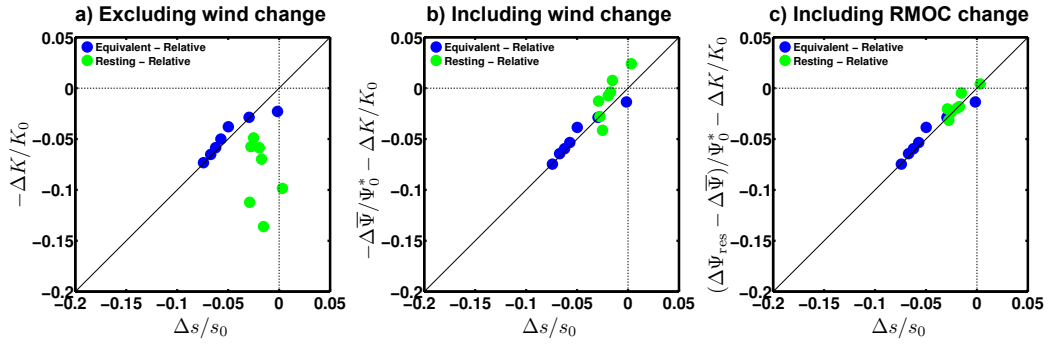


Figure 8: Quantitative tests of residual mean relationship between changes in eddy diffusivity and isopycnal slope. (a) Excluding any wind stress changes, as per Eq. (19), (b) including wind stress changes, but excluding $\Delta\Psi_{res}$, (c) full relationship as per Eq. (18). Blue dots are the difference between the equivalent and relative wind stress experiments, green dots are the difference between the resting ocean and relative wind stress experiments. The dotted lines cross at the origin and the solid line has a gradient of 1.

843 **List of Tables**

844	1	Model Parameters	48
845	2	Key diagnostics of the control experiments. Type of wind 846 stress, Peak wind stress, Domain average EKE, Total circum- 847 polar transport, Bottom transport, Thermal wind transport, 848 Ψ_{upper} , Ψ_{lower} , $\Psi_{\text{m+}}$, $\Psi_{\text{m-}}$	49

Table 1: Model Parameters

Parameter	Symbol	Value	Units
Domain size	L_x, L_y	1000, 1990	km
Latitude of sponge edge	L_{sponge}	1890	km
Domain depth	H	2985	m
Reference density	ρ_0	1000	kg m^{-3}
Thermal expansion coefficient	α	2×10^{-4}	K^{-1}
Coriolis parameter	f_0	-1×10^{-4}	s^{-1}
Gradient in Coriolis parameter	β	1×10^{-11}	$\text{m}^{-1}\text{s}^{-1}$
Surface heat flux magnitude	Q_0	10	W m^{-2}
Control wind speed	U_0	12	m s^{-1}
Bottom drag coefficient	r_b	1.1×10^{-3}	m s^{-1}
Sponge restoring timescale	t_{sponge}	7	days
Sponge vertical scale	h_e	1000	m
Horizontal grid spacing	$\Delta x, \Delta y$	10	km
Vertical grid spacing	Δz	10-250	m
Vertical diffusivity (θ)	κ_v	10^{-5}	$\text{m}^2 \text{s}^{-1}$
Horizontal diffusivity (θ)	κ_h	0	$\text{m}^4 \text{s}^{-1}$
Vertical viscosity (\mathbf{u})	A_v	10^{-3}	$\text{m}^2 \text{s}^{-1}$
Horizontal hyperviscosity (\mathbf{u})	A_4	10^{10}	$\text{m}^4 \text{s}^{-1}$

Table 2: Key diagnostics of the control experiments. Type of wind stress, Peak wind stress, Domain average EKE, Total circumpolar transport, Bottom transport, Thermal wind transport, Ψ_{upper} , Ψ_{lower} , $\Psi_{\text{m+}}$, $\Psi_{\text{m-}}$.

Experiment	τ_0 (Nm $^{-2}$)	EKE (cm 2 s $^{-2}$)	T_{ACC} (Sv)	T_b (Sv)	T_{tw} (Sv)	Ψ_u (Sv)	Ψ_l (Sv)	$\Psi_{\text{m+}}$ (Sv)	$\Psi_{\text{m-}}$ (Sv)
Relative	0.208	43	600	522	78	0.48	-0.29	0.84	-0.49
Equivalent	0.208	50	599	522	77	0.51	-0.28	0.65	-0.47
Resting	0.222	52	629	551	78	0.54	-0.30	0.63	-0.48